Estimating regional flood discharge during Palaeocene-Eocene global warming

Chen Chen[1], Laure Guerit[1,2], Brady Z. Foreman[3], Hima J. Hassenruck-Gudipati[4], Thierry Adatte[5], Louis Honegger[1], Marc Perret[1], Appy Sluijs[6], Sébastien Castelltort[1*]

[1]*Department of Earth Sciences, University of Geneva, Rue des Maraichers 13, 1205 Geneva, Switzerland*

[2]*Géosciences Environnement Toulouse, 14 av. Edouard Belin, 31400 Toulouse, France*

[3]*Department of Geology, Western Washington University, Bellingham, Washington 98225, USA*

[4]*Jackson School of Geosciences, The University of Texas at Austin, 2305 Speedway Stop C1160, Austin, Texas, USA*

[5]*ISTE, Geopolis, University of Lausanne, 1015 Lausanne, Switzerland*

[6]*Department of Earth Sciences, Faculty of Geosciences, Utrecht University, Heidelberglaan 2, 3584CS Utrecht, Netherlands.*

**Corresponding author*

Among the most urgent challenges in future climate change scenarios is accurately predicting the magnitude at which precipitation extremes will intensify. Analogous changes have been reported for an episode of millennial scale 5°C warming termed the Palaeocene-Eocene Thermal Maximum (PETM; 56 Ma), providing independent constraints on hydrological response to global warming. However, quantifying hydrologic extremes during geologic global warming analogs has proven difficult. Here we show that water discharge increased by at least 1.35 and potentially up to 14 times during the PETM in northern Spain. We base these estimates on analyses of channel dimensions, sediment grain size, and palaeochannel gradients across the onset of the PETM, which is regionally marked by an abrupt transition from overbank palaeosol deposits to conglomeratic fluvial sequences. We infer that extreme floods and channel mobility quickly denuded surrounding soil-mantled landscapes, plausibly enhanced by regional vegetation decline, and exported enormous quantities of terrigenous material towards the ocean. These results support hypotheses that extreme rainfall events and associated risks of flooding increase with global warming at similar, but potentially at much higher, magnitudes than currently predicted.

Alluvial deposits within the Tremp-Graus Basin of northern Spain (~35°N palaeolatitude) show a change from strata dominated by overbank palaeosols to an anomalously thick and widespread, conglomeratic fluvial unit that precisely coincides with the early phase of the PETM[1,2]. This was interpreted to reflect the development of a vast braid plain due to an abrupt and dramatic increase in seasonal rainfall[1]. Late Palaeocene floodplain deposits near the town of Aren (Esplugafreda Formation; Fig. 1) are intercalated with coarse sandstones and clast-supported conglomerates filling isolated single- and multi-storey ribbon fluvial channels deposits[4] Levels of gypsum, ubiquitous microcodium remains, abundant carbonate nodule horizons, and reddish palaeosols indicate deposition in generally semi-arid alluvial plains[4,5].

A member of the overlying Claret Formation that formed ~40 kyr prior to the PETM represents a 30 m thick incised valley fill (IVF) made of coarse- and fine-grained fluvial sediment, which displays an erosional base with maximum relief of ~30 m and maximum width of ~5 km[3]. The IVF member is overlaid by an extensive sheet-like clast-supported pebbly calcarenite and conglomerate unit, the Claret Conglomerate (CC), with typical thicknesses of 1 to 4 m and locally up to 8 m[1]. This unit correlates with the onset of the CIE of the PETM (Fig. 1), suggesting the Claret Conglomerate formed over a time span of ~10 kyrs[1]. The CC ends abruptly and is overlaid by ~20 m of fine-grained yellowish soil mainly made up of silty mudstones with abundant small carbonate nodules and gypsum layers, which span the majority of the carbon isotope excursion and its recovery[1]. After the PETM, an interval of red soils marks the return to Palaeocene-like conditions.

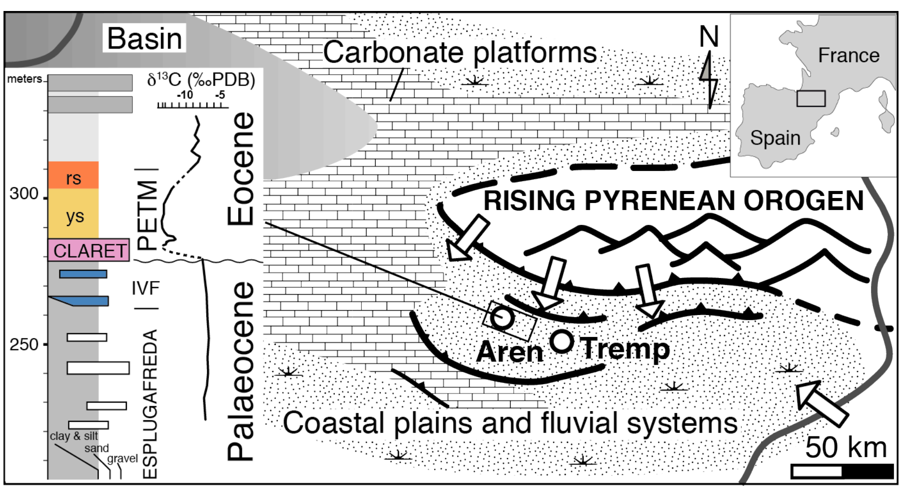

Figure 1 Study area in palaeogeographic context (modified from reference 3) and simplified stratigraphic column with main formations, ages and carbon isotopic profile showing the negative δ13C excursion[1]. IVF:

Incised Valley Fill. PETM: Palaeocene-Eocene Thermal Maximum. ys and rs: yellowish and reddish soils. Arrows indicate main palaeoflow directions in the Late Palaeocene.

To quantify the magnitude of change in water and sediment discharge recorded by the fluvial systems in the basin, we first reconstruct pre-PETM and PETM fluvial palaeoslopes from grain size and channel depth data. We then use palaeoslope and channel width data to invert equilibrium flow velocities and obtain first-order estimates of volumetric discharge during channel forming events before and during the PETM.

We estimated channel depth from fining upward sequences and bar clinoforms[6], and grain size from 26 Palaeocene (Esplugafreda and IVF) and 22 PETM (CC) channel bodies (see Methods, Fig. 2). At each location, the b-axis of between 94 and 405 grains (median of 108), was measured near the base of individual channel deposits (Supplementary Material). D_{50} corresponds to the 50th percentile of the grain size distribution showing a normal cumulative density function. Channel heights are given in meters, with uncertainty of 35% due to incomplete preservation of original channel fill thickness[7].

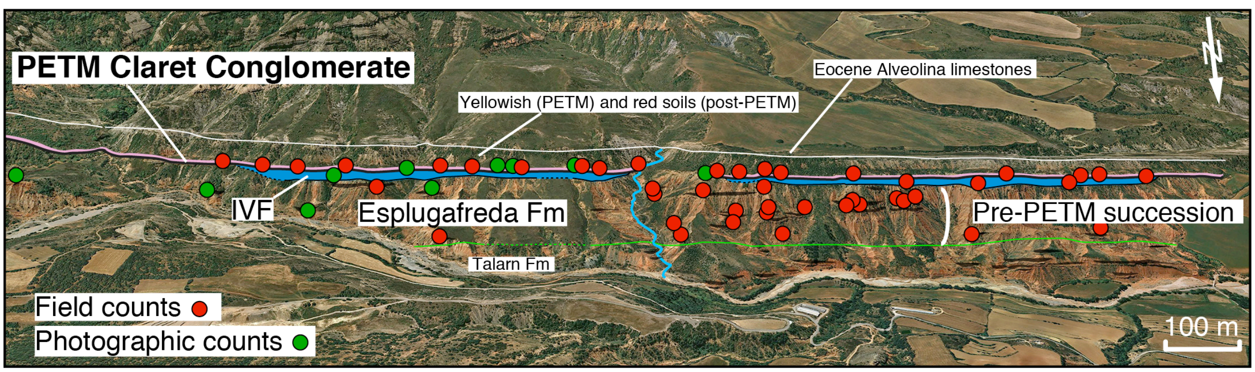

Figure 2 Outcrop panoramic view and line drawing with location of field grain size measurement stations. PETM Claret Conglomerate is in pink above blue IVF interval (colors as on Fig. 1). Green line separates Lower Palaeocene Talarn and Upper Palaeocene Esplugafreda formations. Image data: Google, Digital Globe

The average D_{50} of the pre-PETM is 21.2±5 mm (1σ, N=26) and the average of the CC is 19.5±4 mm (N=22). Average channel depth is 1.1±0.6 m to 1.4±0.6 m, respectively for the Palaeocene and PETM (Fig. 3a). Kruskal-Wallis tests on non-normally distributed grain size (χ^2=1.17, p=0.2791) and channel depth (χ^2=2.97, p=0.085) data do not reject the null hypotheses that Palaeocene and PETM channel deposit have the same median values (at the 5% confidence level).

Paola and Mohrig[8] proposed an estimator of river palaeoslope for coarse-grained braided channel fills S_{est}=0.094×⟨D_{50}⟩/⟨h⟩ (eq. 1, where ⟨D_{50}⟩ and ⟨h⟩ are channel-averaged median grain size and bankfull depth, respectively). Although the Claret Conglomerate appears to meet the specific criteria outlined by Paola and Mohrig[8], the Esplugafreda channels encased in cohesive floodplain banks and interpreted as sinuous ribbons likely do not[4]. Thus, we employ a more generalized empirical relationship for alluvial rivers developed by Trampush[9]: $\log S=\alpha_0+\alpha_1\log D_{50}+\alpha_2\log H_{bf}$ (eq. 2) where S is the channel slope, and H_{bf} the bankfull channel depth. Empirical coefficients, α_0, α_1 and α_2 used are -2.08±0.0015 (mean±standard error SE), 0.2540±0.0007, and -1.0900±0.0019, respectively[9]. Equation 2 is particularly amenable to palaeoslope estimate of both the Esplugafreda and Claret channel deposits because it is based on a broad range of channel patterns, grain size (sand and gravel) and mode of sediment transport. Calculations indicate a decrease in average channel slope from 0.0035±0.0016 (mean±1σ, in m/m) in the Palaeocene to 0.0028±0.0017 during the PETM (Fig. 3b). However, the estimates are not normally distributed and a Kruskal-Wallis test (χ^2=2.22, p=0.136) cannot reject the null hypothesis that the population medians are the same.

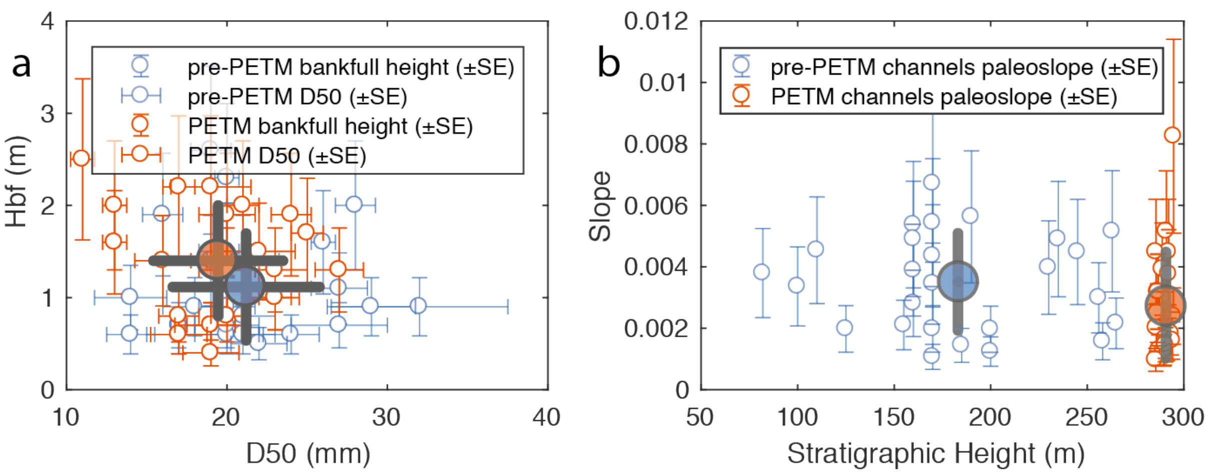

Figure 3 Channel deposits characteristics before and during the PETM global warming. a) D50 and bankfull channel depth Hbf (±SE) at pre-PETM (N=26) and PETM (N=22) field stations. Large circles indicate population mean (± 1σ). b) Calculated palaeoslopes at individual field stations indicated with standard error. Larger circles indicate formation average paleoslope (±1σ).

We estimate volumetric fluxes of water using the average equilibrium flow, U, from Manning's equation ($U=\frac{1}{n}R^{2/3}S^{1/2}$, eq. 3, where n=0.03±0.005 (±1σ) is Manning's coefficient, and R the hydraulic radius is approximated by ⟨h⟩ the channel height) in combination with field estimates of river width. Dreyer and Colombera[4,5] present comprehensive data set of channel width and number of storeys of the Esplugafreda and Claret formations (average palaeoflows are perpendicular to the outcrop strike). Average individual storey width in the Palaeocene is 15±7 m (1σ, N=24, Fig. 4, see Methods) and is interpreted to represent full flow width during channel forming events. In contrast, PETM sandbodies display multi-lateral channels[4,5] that represent belts of shallow interconnected streams with individual storey average width of 169±36 m (1σ, N=13, see Methods and Supplementary Material). Comparison with modern river data (Fig. 4) suggests that active flow widths within such channel belts were most likely near a central value of 95.5 meters, in a range of 22 m to 169 m. The fewer number of total channel bodies in the Claret Conglomerate is related to their larger width compared to the Esplugafreda Formation as the total basin width likely did not change spanning the PETM. Moreover, during the PETM the extreme (close to 100%) channel density prohibits assessments of whether more than one of these braid-belts was active at any given time. In contrast, the very low channel density of ~5% during the Esplugafreda Formation (Fig. 2) suggests only one active channel at a given time. Combining average flow velocity, average channel height and average channel width yields a representative volumetric discharge estimate (±SE) of 31±4.3 m^3/s in the Palaeocene compared to 253±102 m^3/s during the PETM. Propagating uncertainties, this amounts to 8.1±3.5-fold increase (±SE) of volumetric peak channel-forming discharge during the PETM, implying at least a 1.35-fold, and at most a 14.9-fold increase within a 95% confidence interval (±1.96xSE).

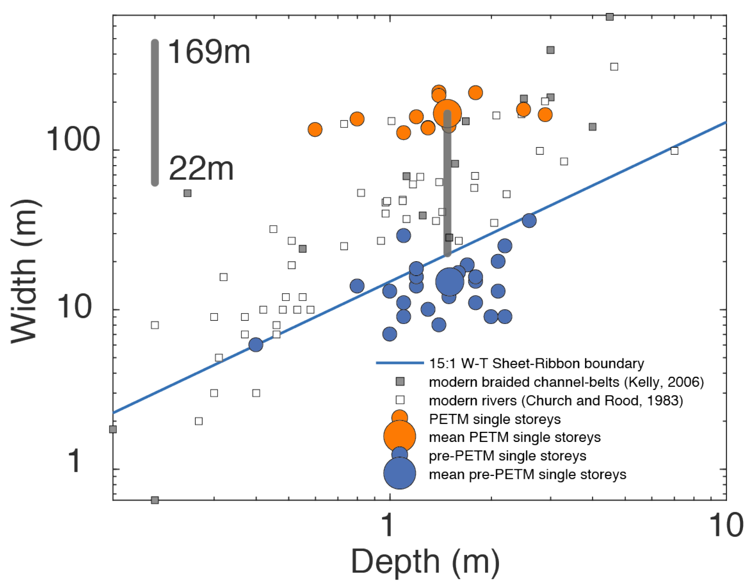

Figure 4 Channel width and depth data recorded before and during the PETM in the Esplugafreda sector. Ribbon channels (width/depth <15) dominate the pre-PETM deposits (blue dots). The range of possible active

flow width during PETM braid-belt deposition is obtained from PETM single-story width estimates (orange dots) and modern river data (white and grey squares).

Channel-forming discharge in alluvial river systems is typically dictated by flood recurrence on timescales of 1.5-3 years[8,10], and slopes adjusted to sediment flux and grain size distribution[11,12]. Therefore the parameters measured in this study unlikely relate to mean annual precipitation conditions, but rather to (inter-) annual rainfall variability and/or extreme precipitation events. These extreme events may be related to transport of the outsized clasts observed by Schmitz and Pujalte[1]. The observed minimal changes in flow depths and slopes, but increases in channel width spanning the PETM are consistent with recent studies that suggest modern, coarse-grained rivers actively self-organize to slightly exceed critical shear velocity under a variety of discharges[13]. Larger floods and discharge events induce channel widening rather than deepening[14].

Likely exacerbating this widening response is the observed vegetation decline in the region. Pollen records of correlative marine sections in western Spain[14] document a change from permanent conifer forests prior to the PETM to sparse vegetation consistent with brief periods of rain in a warmer and drier climate during the PETM. Such a decline in vegetation would have enhanced erodibility of channel banks by decreasing their root-controlled cohesion inducing a more braided planform morphology and/or promoting channel lateral mobility[15]. This behavior would also have enhanced wholesale denudation of the entire landscape. Field studies of deforested/afforested catchments[16] and numerical models of coupled vegetation-landscape evolution[17] demonstrate that devegetated catchments respond quickly to rainfall events and produce narrower hydrographs and higher peak discharges, which result in more-than-linear increase in catchment sediment efflux. The motion of landslides can also be strongly accelerated by even negligible increases in rainfall[18]. Vegetation decline and extreme precipitation events both provide a positive feedback to increased bedload flux, which itself is a primary control on channel cross-sectional aspect ratio[19].

In addition, the observed changes in stratigraphy (abrupt alluvial progradation) are broadly consistent with numerical models of fluvial response to increased mean precipitation rates[11,19,21]. However, since most river adjustment during the PETM took place by enlargement of the braid belt, specific transport capacity does not evolve significantly and thus also implies only minor grain size evolution of the coarse fraction. This phenomenon is also observed in fluvial deposits within the northern Bighorn Basin of Wyoming (U.S.A.), where minimal changes in grain size and flow depths occur, but a combination of seasonal climate, increased sediment flux, and sparse floodplain vegetation generated an anomalously thick and laterally extensive fluvial sandbody[22-24].

Overall our findings contribute to the growing evidence for substantial increases in runoff and continental erosion during the PETM[25,26]. Consistent evidence for hydrological change on land and continental margins further comes from biotic change recorded in fossils[22,27,28], and the hydrogen isotopic composition of plant biomarkers[29]. It appears the PETM caused a number of 'system clearing' events[30] within terrestrial geomorphic systems that flushed fine-grained sediments downstream and were eventually exported into marginal marine settings[23,25,31,32]. A 6-fold and a 9-fold increases in clay abundance across the PETM have been reported in the distal portion of the Tremp-Graus Basin[32] and in the northern margin of the Bay of Biscay[33], respectively. Within error, this is consistent with the vast increase in discharge proposed herein despite the variety of other factors (e.g., marine currents, shelf storage) that control sediment delivery to deep-water[34].

What implications do these results have for the future? Model simulations and observations suggest that anthropogenic climate warming will lead to pronounced changes in global hydrology. Specifically, changes in seasonality and the increased occurrence and intensity of extreme weather events are expected, but uncertainty remains in the magnitude of change[35-37]. Theoretical arguments indicate that precipitation extremes should scale with the water-holding capacity of the atmosphere, which increases at rates of ~7% C^{-1} according to the Clausius–Clapeyron equation[38]. Although this prediction is supported by global data on annual maximum daily rainfall[39], subdaily precipitation extremes (hourly) seem to depart from it[40] with some regions showing lower-than Clausius-Clapeyron scaling while others display "super" Clausius-Clapeyron dependence for temperatures above ~12°C [41] and decreasing rainfall intensity above ~24°C [42]. These predictions, however, may differ significantly between dry and wet regions[37,43], and depend on moisture availability, rainfall mechanism (convective versus stratiform, [44]), and local topographic effects[45] among others. This leads to little consensus on expected perturbations of precipitation patterns with global warming[37].

If we proceed under the presumption that our estimates of river discharges document heavy rainfall events, the observed increase during the PETM warming is at least close to a 7%

C^{-1} Clausius-Clapeyron prediction of 1.4-fold increase for a +5°C of warming (cumulating 7% of increase for 5 warming steps), but likely largely greater than even "super" Clausius-Clapeyron predictions whereby at double the 7% C^{-1} rate[40,41], a +5°C warming yields a 1.93-fold increase in precipitation. Proximity to water masses (Atlantic and Mediterranean) and moisture availability[42], added to local convective and topographic effects in the piedmont of the nascent Pyrenean orogeny could explain such locally amplified response. Within uncertainties, our results suggest a possible "hyper" Clausius-Clapeyron scaling of precipitation extremes during the PETM, and hence support the likelihood that current global warming may intensify extreme rainfall events and associated floods at rates higher, perhaps unpredictably higher, than forecast by general circulation models[40].

METHODS

Grain size data collection

At each location, the b-axis of between 94 and 405 grains (median of 108), were measured near the base of individual channel deposits following established methods[46-48]. The grid-by-number method[49] was used on relatively large, easily accessed outcrops. A grid with regularly spaced nodes was marked over the vertical surface of the outcrop and grains located under each node were measured. The spacing of the nodes was defined according to visual estimate of the D_{90} of the outcrop in order to avoid repeated sampling of identical grains, and on average, nodes were spaced by at least 20 cm. The random method[50] was performed on outcrops with limited extension. In this case, the measured grains were randomly selected in a 1x1 m^2 area. Finally, the grain-size distribution was also determined from pictures for outcrops with access issues[51]. Pictures were taken with a Nikon Coolpix S2700 camera with 16Mpixels resolution from a distance of ca. 1 meter, and a ruler was included on each picture for scale. The average resolution of the pictures thus obtained is ~0.12 mm/pixel. Excluding the edges of the pictures, all visible grains were measured using JMicrovision software [52]. This method corresponds to an areal-by-number sample that must be converted to an equivalent grid-by-number sample to be comparable to other samples. A conversion factor of 2 was used in this study [51,53,54]

Width-depth data

Esplugafreda formation

In the Esplugafreda formation, Dreyer[4] described single- and multistorey ephemeral ribbon-bodies interpreted as arroyo-like channels entrenched into the floodplain, and filled during sporadic discharge episodes. The width and heights of individual storeys within multistorey sandbodies of the Esplugafreda bodies is not reported in Dreyer[4]. The heights of single storeys reported in Dreyer's study range from 0.4 to 5.6 meters. Given our own measures of channel heights, with average of 1.1±0.6m (1σ), we exclude Dreyer's storeys with heights exceeding our measured average by 2 standard deviations (i.e. exceeding 2.25 m), i.e. 6 out of 30 storeys, which we suspect could be multistoreys given their anomalous height. Note that this minimizes the mean channel width taken into account for palaeodischarge estimates by approximately 10%, i.e. mean width of 15±7m (1σ, N=24) instead of 17±8m.

Claret Conglomerate

Channel sandbodies of the Aren exposure drawn in Dreyer[4] allows measuring individual storey dimensions. Dreyer identified single storey sandbodies based on the presence of major erosion surfaces and moderately well developed pedogenesis intervals (pause-planes) between separate bodies. Minor erosion surfaces found *within* the single storeys sandbodies are interpreted as surfaces separating smaller-scale elements *within* a braid-belt such as bars and individual channels[4]. We measured width and depth with reference to Mohrig et al.[6], considering 1) the presence of *wings*, which can represent either a relatively wide topmost internal storey [55], or a channel levee tapering out towards the overbank fines, and 2) the topographic relief above the lowest wing, which can represent either superelevation of the channel above the adjacent floodplain wings[6], or be the result of lateral migration of the entire braid belt. According to Mohrig et al[6], natural channels rarely become superelevated to the point where the riverbed reaches the elevation of the adjacent floodplain. Accordingly, storeys displaying topographic relief (above the lowest wing) greater than incision depth (below the lowest wing) are considered as suspect multistorey channel sandbodies (even though they are identified as single-storey in Dreyer's study) and excluded from the analysis. Width and depth of sandbodies are therefore measured at the level of the lowest wing, or at the level of the lowest eroded sandbody margin (Supplementary Figure 1), thus always yielding conservative width estimates. According to this approach, the average single-storey width estimated amounts to a conservative value of 169±36m (1σ, N=13). By comparison, Colombera et al [11] recently described the entire multistorey channel complexes of the Claret formation and measured an average width of 484±508m (1σ).

Church and Rood (1983) river data

Figure 4 shows the width and depth of modern rivers of the Church and Rood[56] catalogue with median grain size in the same range as found in the Esplugafreda and Claret deposits (17.5 mm to 27 mm).

Clausius-Clapeyron changes in precipitation

Precipitation extremes are expected to scale with temperature change at a rate given by the Clausius-Clapeyron equation, which governs change in water-holding capacity of the atmosphere at a rate of 7% per degree[38]. Cumulating this rate 5 times to account for a 5°C increase in temperature during the PETM amounts to a ~40% increase in precipitation, i.e. 1.4 times the initial pre-PETM value. So-called "super" Clausius-Clapeyron scaling involves a doubling (i.e. 14%) of the above rate for average temperatures above 12°C, which implies a 1.93-fold increase in precipitation from initial value for a 5°C global warming.

Acknowledgements

This research was funded by Swiss National Science Foundation grant Earth Surface Signaling Systems to S.C (No 200021-146822). A.S. acknowledges support from the Netherlands Earth System Sciences Centre (NESSC). We acknowledge Chris Paola, Fritz Schlunegger and David Mohrig for discussions.

Author Contributions

C.C., L.G., B.Z.F., H.J.H., T.A., L.H., M.P. and S.C. collected field data. C.C., L.G., B.Z.F. and S.C. supervised field data collection, statistical analyses and palaeohydraulic estimates. S.C. wrote the manuscript with A.S., B.Z.F., C.C. and L.G. All authors contributed to data analysis, interpretation, manuscript editing and discussions.

Competing Financial Interests statement

The authors declare no competing financial interests.

References

1 Schmitz, B. & Pujalte, V. Abrupt increase in seasonal extreme precipitation at the Palaeocene-Eocene boundary. *Geology* **35**, 215-218 (2007).

2 Schmitz, B. & Pujalte, V. Sea-level, humidity, and land-erosion records across the initial Eocene thermal maximum from a continental-marine transect in northern Spain. *Geology* **31**, 689, doi:10.1130/g19527.1 (2003).

3 Pujalte, V., Schmitz, B. & Baceta, J. I. Sea-level changes across the Palaeocene–Eocene interval in the Spanish Pyrenees, and their possible relationship with North Atlantic magmatism. *Palaeogeography, Palaeoclimatology, Palaeoecology* **393**, 45-60, doi:10.1016/j.palaeo.2013.10.016 (2014).

4 Dreyer, T. Quantified fluvial architecture in ephemeral stream deposits of the Esplugafreda Formation (Palaeocene), Tremp-Graus Basin, northern Spain. In *Alluvial Sedimentation*, edited by Marzo, M and Puigdefabregas, C. *Spec. Publs Int. Ass. Sediment.* **17**, 337-362 (1993).

5 Colombera, L., Arévalo, O. J. & Mountney, N. P. Fluvial-system response to climate change: The Palaeocene-Eocene Tremp Group, Pyrenees, Spain. *Global and Planetary Change* **157**, 1-17 (2017).

6 Mohrig, D., Heller, P. L., Paola, C. & Lyons, W. J. *Geological Society of America Bulletin* **112**, 1787, doi:10.1130/0016-7606(2000)112<1787:iapfaa>2.0.co;2 (2000).

7 Paola, C. & Borgman, L. Reconstructing random topography from preserved stratification. *Sedimentology* **38**, 553-565 (1991).

8 Paola, C. & Mohrig, D. Palaeohydraulics revisited: palaeoslope estimation in coarse-grained braided rivers. *Basin Research* **8**, 243-254 (1996).

9 Trampush, S. M., Huzurbazar, S. & McElroy, B. Empirical assessment of theory for bankfull characteristics of alluvial channels. *Water Resources Research* **50**, 9211-9220, doi:10.1002/2014wr015597 (2014).

10 Castro, J. M. & Jackson, P. L. Bankfull discharge recurrence intervals and regional hydraulic geometry relationships: Patterns in the Pacific Northwest, USA. *JAWRA Journal of the American Water Resources Association* **37**, 1249-1262 (2001).

11 Paola, C., Heller, P. L. & Angevine, C. L. The large-scale dynamics of grain-size variation in alluvial basins, 1: Theory. *Basin Research* **4**, 73-90 (1992).

12 Fedele, J. J. & Paola, C. Similarity solutions for fluvial sediment fining by selective deposition. *Journal of Geophysical Research* **112**, doi:10.1029/2005jf000409 (2007).

13 Phillips, C. B. & Jerolmack, D. J. Self-organization of river channels as a critical filter on climate signals. *Science* **352**, 694-697 (2016).

14 Schmitz, B., Pujalte, V. & Nunez-Betelu, K. Climate and sea-level perturbations during the Incipient Eocene Thermal Maximum: evidence from siliciclastic units in the Basque Basin (Ermua, Zumaia and Trabakua Pass), northern Spain. *Palaeogeography, Palaeoclimatology, Palaeoecology* **165**, 299-320 (2001).

15 Gran, K. & Paola, C. Riparian vegetation controls on braided stream dynamics. *Water Resources Research* **37**, 3275-3283 (2001).

16 Alatorre, L., Beguería, S., Lana-Renault, N., Navas, A. & García-Ruiz, J. Soil erosion and sediment delivery in a mountain catchment under scenarios of land use change using

a spatially distributed numerical model. *Hydrology and Earth System Sciences* **16**, 1321 (2012).

17 Coulthard, T., Kirkby, M. & Macklin, M. Modelling geomorphic response to environmental change in an upland catchment. *Hydrological Processes* **14**, 2031-2045 (2000).

18 Schulz, W. H. *et al.* Landslide kinematics and their potential controls from hourly to decadal timescales: Insights from integrating ground-based InSAR measurements with structural maps and long-term monitoring data. *Geomorphology* **285**, 121-136 (2017).

19 Métivier, F. & Barrier, L. Alluvial Landscape Evolution: What Do We Know About Metamorphosis of Gravel-Bed Meandering and Braided Streams? *Gravel-bed Rivers: processes, tools, environments*, 474-501 (2012).

20 Armitage, J. J., Duller, R. A., Whittaker, A. C. & Allen, P. A. Transformation of tectonic and climatic signals from source to sedimentary archive. *Nature Geoscience* **4**, 231-235 (2011).

21 Simpson, G. & Castelltort, S. Model shows that rivers transmit high-frequency climate cycles to the sedimentary record. *Geology* **40**, 1131-1134 (2012).

22 Wing, S. L. *et al.* Transient floral change and rapid global warming at the Palaeocene-Eocene boundary. *Science* **310**, 993-996 (2005).

23 Foreman, B. Z. Climate-driven generation of a fluvial sheet sand body at the Palaeocene-Eocene boundary in north-west Wyoming (USA). *Basin Research* **26**, 225-241, doi:10.1111/bre.12027 (2014).

24 Kraus, M. J., Woody, D. T., Smith, J. J. & Dukic, V. Alluvial response to the Palaeocene–Eocene Thermal Maximum climatic event, Polecat Bench, Wyoming (USA). *Palaeogeography, Palaeoclimatology, Palaeoecology* **435**, 177-192 (2015).

25 Sluijs, A. *et al.* Warming, euxinia and sea level rise during the Palaeocene-Eocene Thermal Maximum on the Gulf Coastal Plain: Implications for ocean oxygenation and nutrient cycling. *Climate of the Past* **10**, 1421 (2014).

26 Carmichael, M. J. *et al.* Hydrological and associated biogeochemical consequences of rapid global warming during the Palaeocene-Eocene Thermal Maximum. *Global and Planetary Change* **157**, 114-138 (2017).

27 Sluijs, A. & Brinkhuis, H. A dynamic climate and ecosystem state during the Palaeocene-Eocene Thermal Maximum: inferences from dinoflagellate cyst assemblages on the New Jersey Shelf. *Biogeosciences* **6** (2009).

28 Eldrett, J., Greenwood, D., Polling, M., Brinkhuis, H. & Sluijs, A. A seasonality trigger for carbon injection at the Palaeocene–Eocene Thermal Maximum. *Climate of the Past* **10**, 759-769 (2014).

29 Pagani, M. *et al.* Arctic hydrology during global warming at the Palaeocene/Eocene thermal maximum. *Nature* **442**, 671-675 (2006).

30 Jerolmack, D. J. & Paola, C. Shredding of environmental signals by sediment transport. *Geophysical Research Letters* **37** (2010).

31 Foreman, B. Z., Heller, P. L. & Clementz, M. T. Fluvial response to abrupt global warming at the Palaeocene/Eocene boundary. *Nature* **491**, 92-95 (2012).

32 Bolle, M., Adatte, T., Keller, G., Von Salis, K. & Hunziker, J. Biostratigraphy, mineralogy and geochemistry of the Trabakua Pass and Ermua sections in Spain: Palaeocene-Eocene transition. (1998).

33 Bornemann, A. *et al.* Persistent environmental change after the Palaeocene–Eocene Thermal Maximum in the eastern North Atlantic. *Earth and Planetary Science Letters* **394**, 70-81 (2014).

34 Covault, J. A. & Graham, S. A. Submarine fans at all sea-level stands: Tectono-morphologic and climatic controls on terrigenous sediment delivery to the deep sea. *Geology* **38**, 939-942 (2010).

35 Coumou, D. & Rahmstorf, S. A decade of weather extremes. *Nature climate change* **2**, 491-496 (2012).

36 Edenhofer, O. *et al.* IPCC, 2014: summary for policymakers. *Climate change* (2014).

37 Donat, M. G., Lowry, A. L., Alexander, L. V., O'Gorman, P. A. & Maher, N. More extreme precipitation in the world's dry and wet regions. *Nature Climate Change* **6**, 508-513 (2016).

38 Trenberth, K. E., Dai, A., Rasmussen, R. M. & Parsons, D. B. The changing character of precipitation. *Bulletin of the American Meteorological Society* **84**, 1205-1217 (2003).

39 Westra, S., Alexander, L. V. & Zwiers, F. W. Global increasing trends in annual maximum daily precipitation. *Journal of Climate* **26**, 3904-3918 (2013).

40 Westra, S. *et al.* Future changes to the intensity and frequency of short-duration extreme rainfall. *Reviews of Geophysics* **52**, 522-555 (2014).

41 Lenderink, G. & Van Meijgaard, E. Increase in hourly precipitation extremes beyond expectations from temperature changes. *Nature Geoscience* **1**, 511-514 (2008).

42 Hardwick Jones, R., Westra, S. & Sharma, A. Observed relationships between extreme sub-daily precipitation, surface temperature, and relative humidity. *Geophysical Research Letters* **37** (2010).

43 Byrne, M. P. & O'Gorman, P. A. The response of precipitation minus evapotranspiration to climate warming: Why the "wet-get-wetter, dry-get-drier" scaling does not hold over land. *Journal of Climate* **28**, 8078-8092 (2015).

44 Berg, P., Moseley, C. & Haerter, J. O. Strong increase in convective precipitation in response to higher temperatures. *Nature Geoscience* **6**, 181-185 (2013).

45 Siler, N. & Roe, G. How will orographic precipitation respond to surface warming? An idealized thermodynamic perspective. *Geophysical Research Letters* **41**, 2606-2613 (2014).

SUPPLEMENTARY MATERIAL

Manuscript title:

Estimating regional flood discharge during Palaeocene-Eocene global warming

Authors:

Chen Chen[1], Laure Guerit[1,2], Brady Z. Foreman[3], Hima J. Hassenruck-Gudipati[4], Thierry Adatte[5], Louis Honegger[1], Marc Perret[1], Appy Sluijs[6], Sébastien Castelltort[1*]

[1]Department of Earth Sciences, University of Geneva, Rue des Maraichers 13, 1205 Geneva, Switzerland

[2]Géosciences Environnement Toulouse, 14 av. Edouard Belin, 31400 Toulouse, France

[3]Department of Geology, Western Washington University, Bellingham, Washington 98225, USA

[4]Jackson School of Geosciences, The University of Texas at Austin, 2305 Speedway Stop C1160, Austin, Texas, USA

[5]ISTE, Geopolis, University of Lausanne, 1015 Lausanne, Switzerland

[6]Department of Earth Sciences, Faculty of Geosciences, Utrecht University, Heidelberglaan 2, 3584CS Utrecht, Netherlands.

**Corresponding author*

1. Supplementary Table 1: grain size and channel height data

Supplemental file "Chen_Supplementary_Table_1.pdf". Median grain size and channel height data of field stations with their geolocalisation.

2. Supplementary Figure 1

Panoramic view of single storey conglomeratic bodies of the Claret formation in the sector of Aren (redrawn from reference 10) with indications of width and height measurements.

3. Supplementary Table 2: width-depth data

Supplemental file with measurements of width-depth data measured from Supplementary Figure 1 (Claret Conglomerate) and obtained from ref 10 (pre-PETM Esplugafreda formation).

4. Bibliographic references of the Method section

46 Church, M. A., McLean, D. & Wolcott, J. River bed gravels: sampling and analysis. *Sediment Transport in Gravel-Bed Rivers. John Wiley and Sons New York. 1987. p 43-88, 17 fig, 3 tab, 50 ref.* (1987).

47 Diplas, P. & Fripp, J. B. Properties of various sediment sampling procedures. *Journal of Hydraulic Engineering* **118**, 955-970 (1992).
48 Rice, S. & Church, M. Sampling surficial fluvial gravels: the precision of size distribution percentile estimates. *Journal of Sedimentary Research* **66** (1996).
49 Wolman, M. G. A method of sampling coarse river-bed material. *EOS, Transactions American Geophysical Union* **35**, 951-956 (1954).
50 Bevenger, G. S. & King, R. M. A pebble count procedure for assessing watershed cumulative effects. *Research paper RM (USA)* (1995).
51 Bunte, K. & Abt, S. R. Sampling surface and subsurface particle-size distributions in wadable gravel-and cobble-bed streams for analyses in sediment transport, hydraulics, and streambed monitoring. (2001).
52 Roduit, N. JMicroVision: Image analysis toolbox for measuring and quantifying components of high-definition images. *Ver* **1**, 2002-2007 (2008).
53 Kellerhals, R. & Bray, D. I. Sampling procedures for coarse fluvial sediments. *Journal of the Hydraulics Division* **97**, 1165-1180 (1971).
54 Graham, D. J., Rollet, A.-J., Rice, S. P. & Piégay, H. Conversions of surface grain-size samples collected and recorded using different procedures. *Journal of Hydraulic Engineering* **138**, 839-849 (2012).
55 Gibling, M. R. Width and Thickness of Fluvial Channel Bodies and Valley Fills in the Geological Record: A Literature Compilation and Classification. *Journal of Sedimentary Research* **76**, 731-770, doi:10.2110/jsr.2006.060 (2006).
56 Church, M. and Rood, K. Catalogue of alluvial river channel regime data. The University of British Columbia, Department of Geography, Vancouver. (1983).

Estimating regional flood discharge during Palaeocene-Eocene global warming

Chen Chen, Laure Guerit, Brady Z. Foreman, Hima J. Hassenruck-Gudipati, Thierry Adatte, Louis Honegger, Marc Perret, Appy Sluijs, Sébastien Castelltort

SUPPLEMENTARY TABLE 1: CHANNEL HEIGHT AND GRAIN SIZE

D50=median grain diameter
STD=Standard Deviation
SE=Standard Error

PETM CLARET CONGLOMERATE

n	Channel height	35% SE (m)	D50	STD (mm)	SE (mm)	Latitude	Longitude
102	1	0.35	23	13	1.5	42.24667	0.74591
112	1.9	0.665	20	16	1.75	42.24466	0.76286
110	2.2	0.77	19	26	2.5	42.24429	0.76446
113	1.3	0.455	20	17	1.75	42.24521	0.75899
109	1.5	0.525	22	21	2.25	42.24504	0.75991
105	0.4	0.14	19	16	1.75	42.24537	0.75756
115	0.7	0.245	19	22	2.25	42.24537	0.75558
120	0.8	0.28	20	10	1	42.24543	0.75507
119	1.4	0.49	16	17	1.75	42.24625	0.75154
106	1.3	0.455	27	15	1.5	42.2465	0.7501
113	0.8	0.28	17	11	1.25	42.24716	0.73998
110	0.7	0.245	19	15	1.5	42.24681	0.74743
106	0.6	0.21	17	17	1.75	42.24658	0.74957
102	1.3	0.455	23	20	2	42.245	0.75374
205	1.7	0.595	25	12	1	42.24540	0.75576
171	2	0.7	13	7	0.75	42.24515	0.75803
209	1	0.35	23	13	1	42.24515	0.75803
102	2.2	0.77	17	8	1	42.24515	0.75803
96	2.5	0.875	11	7	0.75	42.24619	0.75186
188	1.6	0.56	13	7	0.75	42.24468	0.76104
104	1.9	0.665	24	11	1.25	42.24468	0.76104
210	2	0.7	21	12	1	42.24417	0.77308

PRE-PETM ESPLUGAFREDA AND IVF FORMATIONS

n	Channel height	35% SE (m)	D50	STD (mm)	SE (mm)	Latitude	Longitude
103	0.6	0.21	17	18	2	42.24723	0.74092
113	1.4	0.49	21	23	2.25	42.24709	0.74371
100	1.1	0.385	27	16	1.75	42.2469	0.74586
98	0.7	0.245	27	28	3	42.24467	0.7633
100	0.9	0.315	32	54	5.5	42.24665	0.75201
108	0.8	0.28	21	19	2	42.24747	0.75021
110	0.6	0.21	24	17	1.75	42.24522	0.76186
103	0.6	0.21	20	18	2	42.24608	0.75347
110	0.6	0.21	14	15	1.5	42.24744	0.74911
107	0.5	0.175	22	17	1.75	42.24755	0.74786
107	1	0.35	14	21	2.25	42.24749	0.74768
104	0.9	0.315	20	17	1.75	42.24761	0.7475
101	1.5	0.525	20	17	1.75	42.24747	0.74641
104	0.6	0.21	21	18	2	42.24757	0.74621
105	0.7	0.245	20	18	2	42.24747	0.74583
102	0.9	0.315	29	27	2.75	42.24877	0.74065
101	0.7	0.245	19	13	1.5	42.248	0.75291
101	1.4	0.49	19	11	1.25	42.24685	0.75101
100	0.9	0.315	18	19	2	42.24756	0.75021
208	2	0.7	28	17	1.25	42.24811	0.74999
406	1.5	0.525	20	12	0.75	42.24575	0.764
308	1.6	0.56	26	12	0.75	42.24563	0.76016
205	2.3	0.805	20	10	0.75	42.24563	0.76016
301	0.7	0.245	17	8	0.5	42.24458	0.76735
100	2.6	0.91	19	11	1.25	42.24417	0.78084
98	1.9	0.665	16	11	1.25	42.24804	0.73949

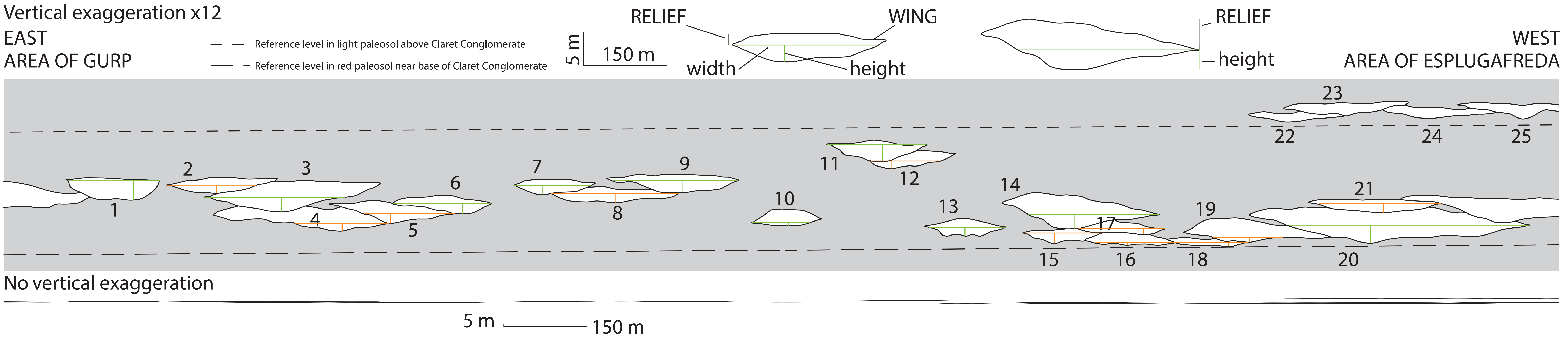

SUPPLEMENTARY FIGURE 1

Estimating regional flood discharge during Palaeocene-Eocene global warming

Chen Chen, Laure Guerit, Brady Z. Foreman, Hima J. Hassenruck-Gudipati, Thierry Adatte, Louis Honegger, Marc Perret, Appy Sluijs, Sébastien Castelltort

SUPPLEMENTARY TABLE 2: WIDTH AND DEPTH OF CONGLOMERATIC BODIES

CLARET CONGLOMERATE - measurements and storey numbers refer to bodies of Supplementary Figure 1

Storey	Thickness (mm)	Width (mm)	T (m)	W (m)	Storey type	
1	7.635	35.748	2.9	166	single	considered
2	3.234	34.807	1.2	161	single-eroded	considered
3	5.647	54.316	2.2	252	multiple	not considered
4	2.973	36.167	1.1	168	multiple	not considered
5	3.701	34.984	1.4	162	multiple-eroded	not considered
6	3.887	38.136	1.5	177	single	considered
7	3.452	29.81	1.3	138	single	considered
8	3.531	49.689	1.4	230	single-eroded	considered
9	4.694	49.198	1.8	228	single	considered
10	1.279	22.622	0.5	105	multiple	not considered
11	6.499	38.644	2.5	179	single	considered
12	2.969	27.512	1.1	128	single-eroded	considered
13	3.444	29.501	1.3	137	single	considered
14	5.473	50.594	2.1	235	multiple	not considered
15	3.98	30.462	1.5	141	single-eroded	considered
16	0.902	31.24	0.3	145	multiple-eroded	not considered
17	2.16	33.676	0.8	156	single-eroded	considered
18	1.653	28.862	0.6	134	single-eroded	considered
19	1.927	27.258	0.7	126	multiple-eroded	not considered
20	6.986	93.188	2.7	432	multiple	not considered
21	3.597	47.155	1.4	219	single-eroded	considered

ESPLUGAFREDA SINGLE-STOREY RIBBON BODIES

Data from Dreyer (1993), Figure 9, Panel D

Thickness (m)	Width (m)	
0.4	6	considered
1	7	considered
1.1	9	considered
1.4	8	considered
1.3	10	considered
1.1	11	considered
1	13	considered
0.8	14	considered
1.2	14	considered
1.2	16	considered
1.2	18	considered
1.1	29	considered
1.7	19	considered
1.6	17	considered
1.5	12	considered
1.8	11	considered
2	9	considered
2.2	9	considered
2.1	13	considered
1.8	15	considered
1.8	16	considered
2.1	20	considered
2.2	25	considered
2.6	36	considered
3.1	26	not considered
3.2	16	not considered
3.6	26	not considered
4.4	18	not considered
5.1	23	not considered
5.6	37	not considered